eLIFE
elifesciences.org

Figures and figure supplements

c-di-GMP heterogeneity is generated by the chemotaxis machinery to regulate flagellar motility

Bridget R Kulasekara, et al.

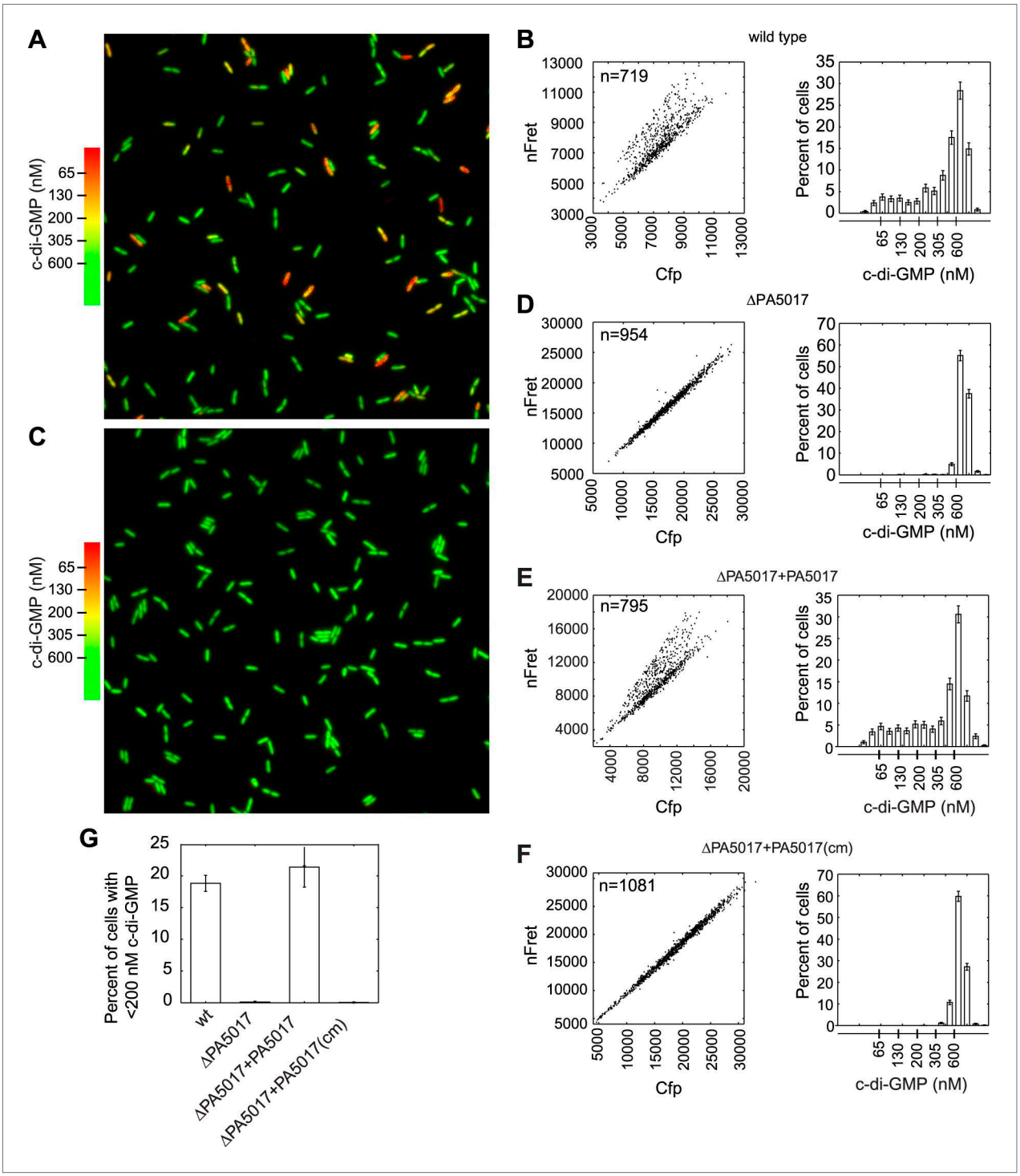

Figure 1. PA5017/*pch* is required for heterogeneity in c-di-GMP levels. (**A**) Wild-type *P. aeruginosa* cells exhibit heterogeneity in c-di-GMP levels. Pseudocolored nFret/Cfp ratios from a single field (88.7 × 88.7 microns) demonstrate c-di-GMP concentrations in wild-type *P. aeruginosa* PA14 cells. (**B**) Quantification of cellular c-di-GMP levels in wild-type *P. aeruginosa* cells. The left panel shows a scatter plot of the mean nFret vs Cfp values in individual cells. In the right panel is a histogram of the corresponding cellular c-di-GMP levels where error bars depict the counting error. Graphs in (**D**), (**E**), and (**F**) assume the same format. (**C**) c-di-GMP concentrations in the PA5017 deletion. (**D**) Quantification of c-di-GMP concentrations in ΔPA5017 cells. (**E**) Quantification of c-di-GMP concentrations in ΔPA5017 complemented with PA5017. (**F**) Quantification of c-di-GMP concentrations in ΔPA5017 complemented with a catalytic mutant (cm) of PA5017. (**G**) Quantification of the mean percentage of cells with less than 200 nM c-di-GMP from three biological replicates. Error bars depict the standard deviation.

DOI: 10.7554/eLife.01402.003

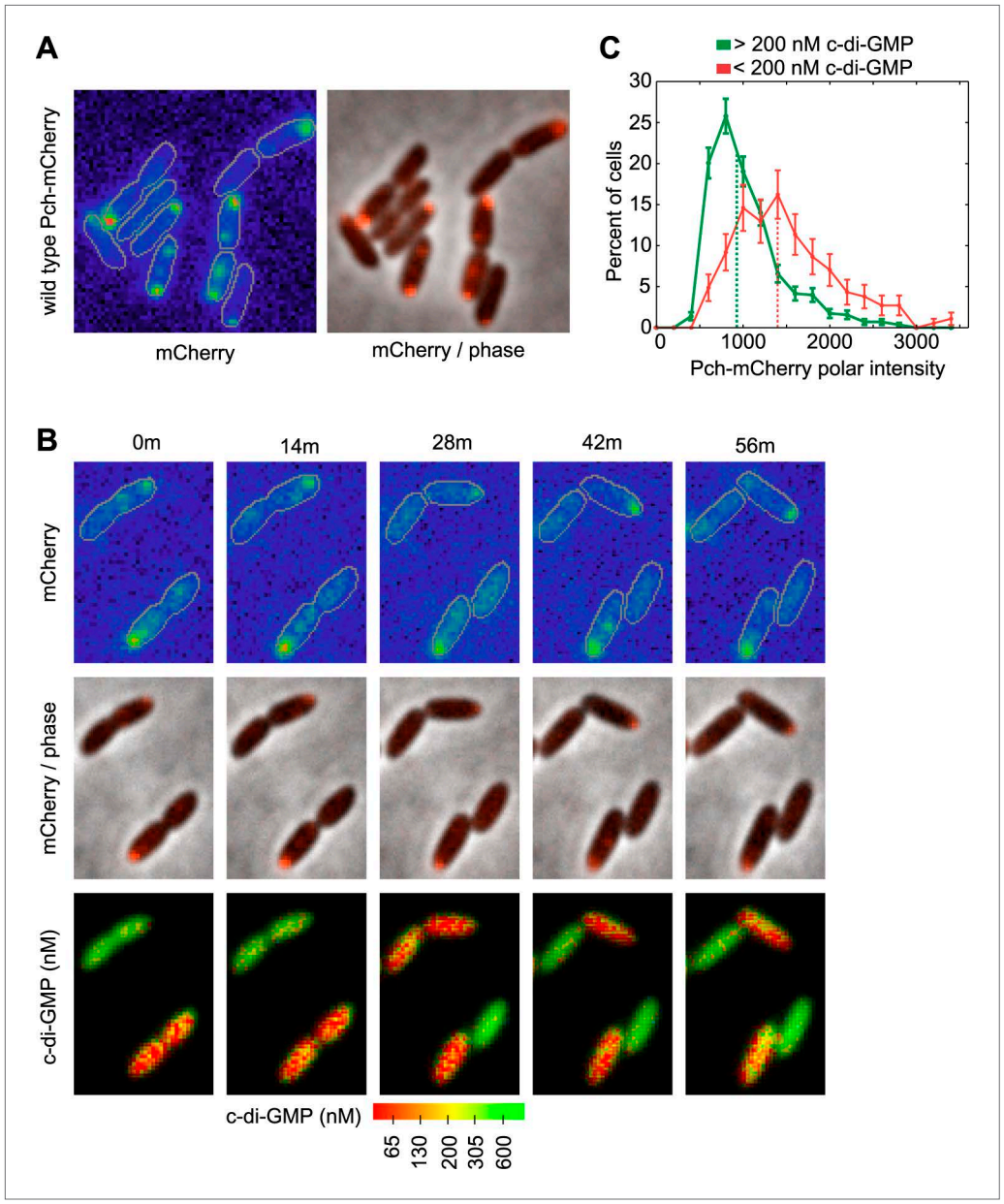

Figure 2. Pch localizes to the cell pole and is asymmetrically partitioned to generate heterogeneity in cellular c-di-GMP levels. (**A**) A representative image (10.8 × 10.8 microns) of Pch-mCherry subcellular localization. The fluorescence channel (mCherry) on the left illustrates the range of subcellular concentrations of Pch-mCherry. A rainbow color map was utilized to represent different intensity values. Red represents the highest intensity and purple represents the lowest intensity. Cell boundaries are delineated in gray. An overlay of the fluorescence channel (in red) and the phase contrast image on the right, illustrates the predominant Pch-mCherry subcellular localization pattern. Refer to the 'Materials and methods' section for a description of contrast settings for both image types. (**B**) Polar localization of Pch-mCherry is associated with low cellular c-di-GMP after cell division, as shown by representative time-lapse images (width of 6.3 microns) of biosensor activity and Pch-mCherry localization in two dividing cells. The top panel is of the fluorescence image. The middle panel contains an overlay of the fluorescence channel (in red) and the phase contrast image. The bottom panel displays pseudocolored nFret/Cfp values that depict c-di-GMP concentrations. (**C**). Distribution of the mean polar Pch-mCherry intensity of 797 cells binned according to c-di-GMP. Polar intensity has been plotted for the cell pole with the greatest intensity. Dotted lines mark the median values. Error bars depict the counting error.

DOI: 10.7554/eLife.01402.004

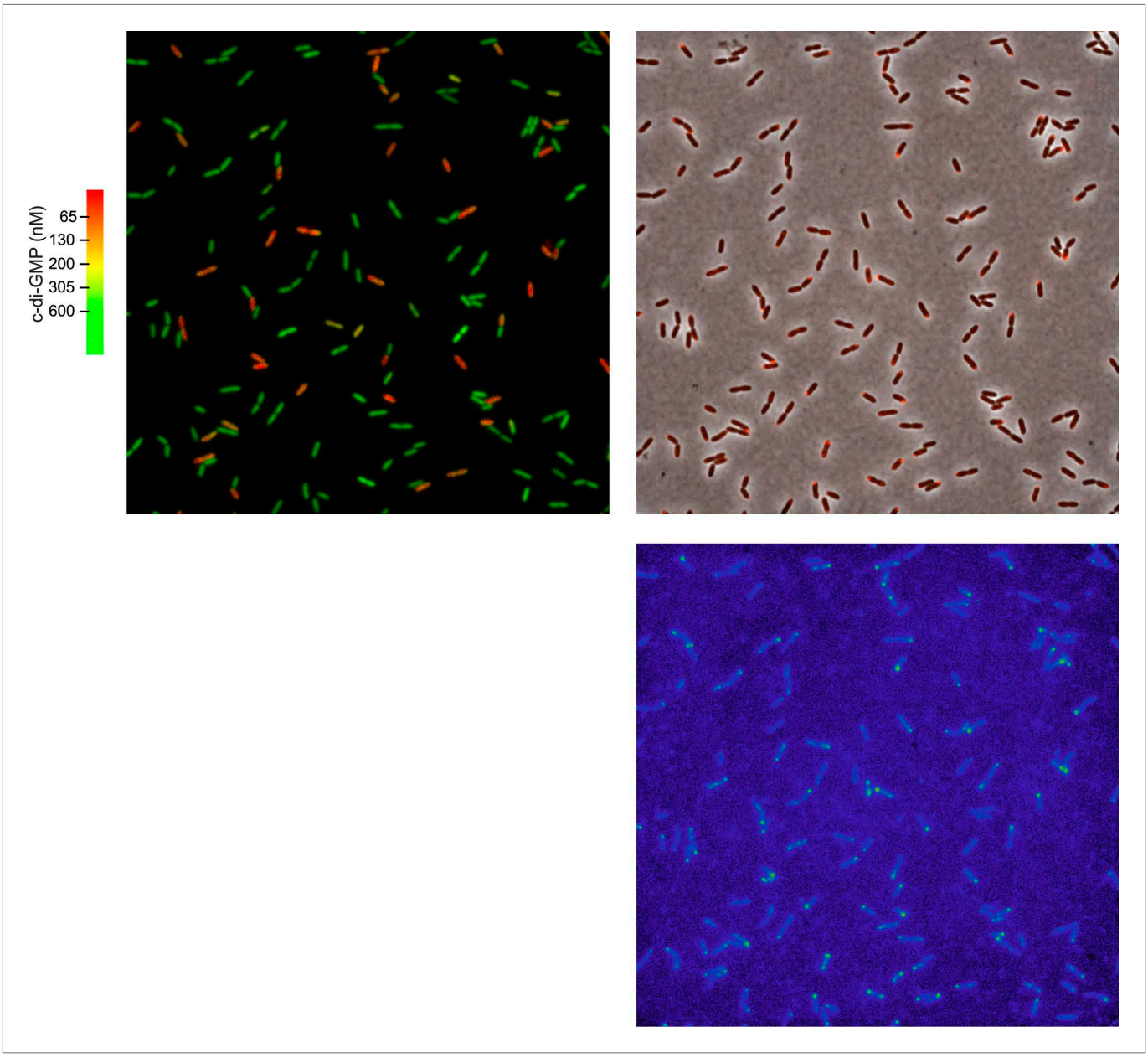

Figure 2—figure supplement 1. Polar localization of Pch-mCherry is associated with lower cellular c-di-GMP. One field (88.7 × 88.7 microns) used to generate ***Figure 2C***. The left panel is of a pseudocolored nFret/Cfp image demonstrating c-di-GMP levels. The right panel is an overlay of the phase contrast image and fluorescence image (red) of Pch-mCherry. The bottom panel is of the fluorescence image. A rainbow color map has been utilized to represent intensity values.

DOI: 10.7554/eLife.01402.005

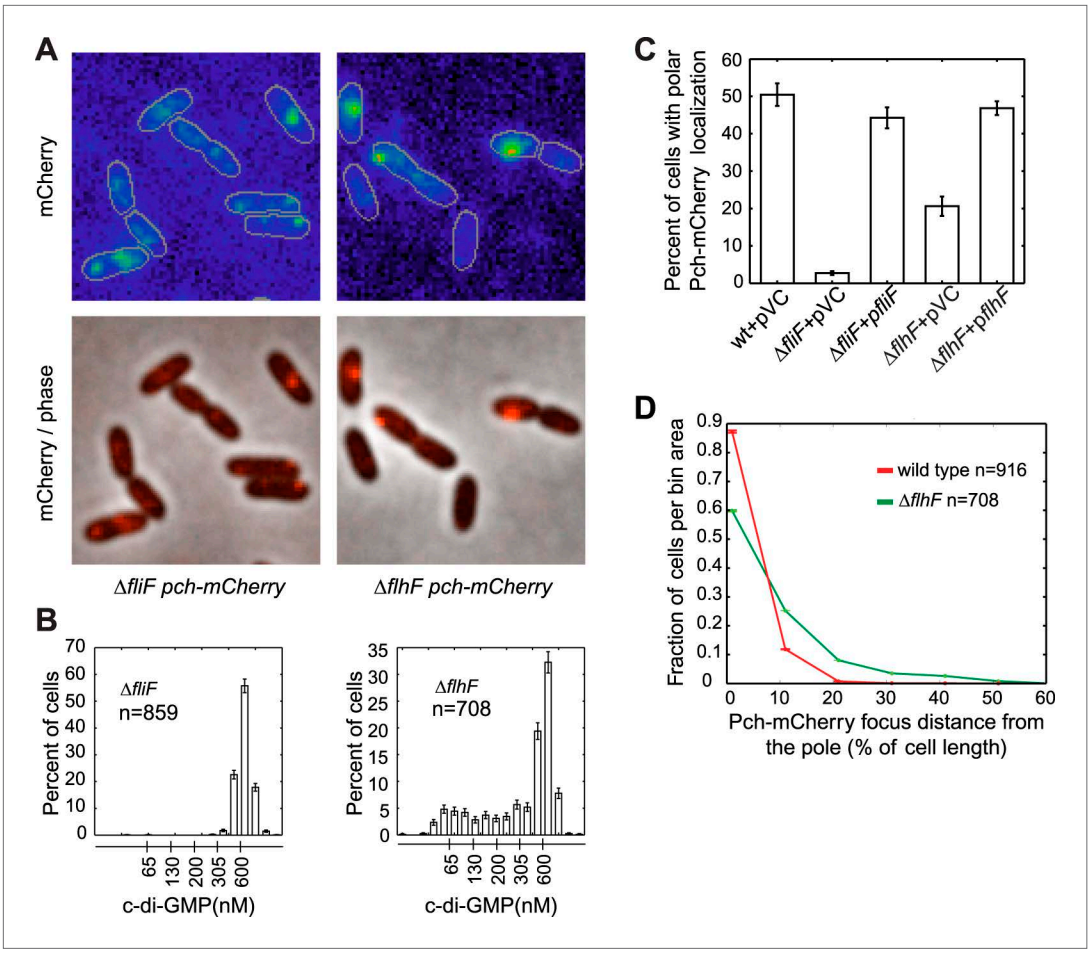

Figure 3. The flagellar apparatus is required for Pch polar localization and maintenance of low c-di-GMP. (**A**) Representative images (10.8 × 10.8 microns) of Pch-mCherry localization in *fliF* and *flhF* deletions. Refer to the 'Materials and methods' section for a description of contrast settings for both image types. (**B**) Histograms of cellular c-di-GMP concentrations in *fliF* and *flhF* deletions. Error bars represent counting error. The mean percentage of Δ*fliF* cells with less than 200 nM c-di-GMP from three biological replicates is 0.1% (standard deviation of 0.1%). The mean percentage of Δ*flhF* cells with less than 200 nM c-di-GMP from three biological replicates is 26.6% (standard deviation of 5.2%). (**C**) Quantification of the mean percentage of cells exhibiting polar localization of Pch-mCherry in Δ*fliF* and Δ*flhF* backgrounds from four biological replicates. Error bars represent the standard deviation. Strains contain empty vector (pVC) or a complementing plasmid. Quantification was performed as described in the 'Materials and methods'. (**D**) A representative histogram of Pch-mCherry focus distance to the nearest cell pole in wild type and *flhF* deletion strains. Error bars depict counting error.

DOI: 10.7554/eLife.01402.006

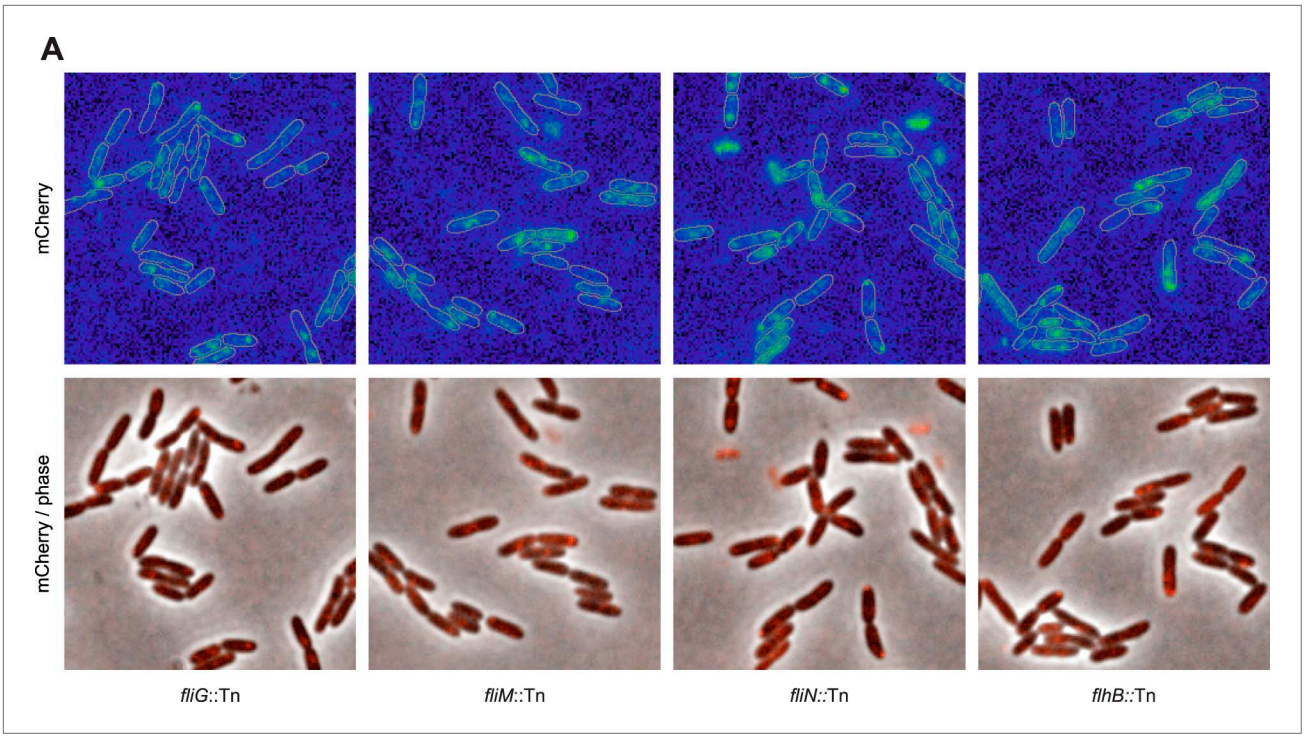

Figure 3—figure supplement 1. The flagellar apparatus is required for Pch-mCherry polar localization. Representative images (21.7 × 21.7 microns) of Pch-mCherry subcellular localization in transposon insertion mutants of the flagellar rotor and export apparatus in *P. aeruginosa* PAO1.
DOI: 10.7554/eLife.01402.007

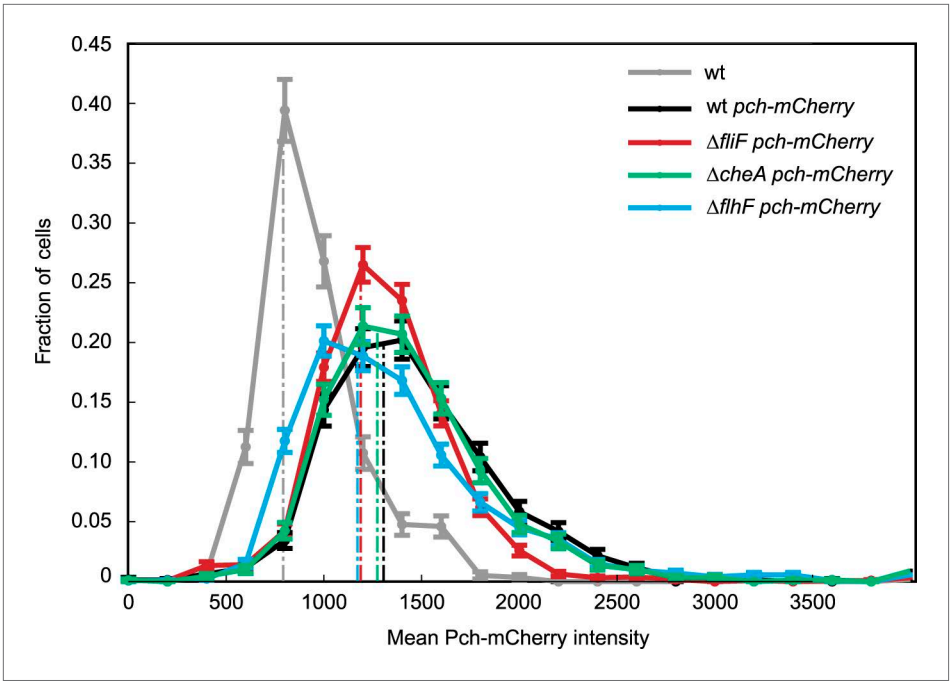

Figure 3—figure supplement 2. Quantitation of Pch. A representative histogram of mean cellular intensity of Pch-mCherry in different strain backgrounds. Median values are marked by dotted lines.

DOI: 10.7554/eLife.01402.008

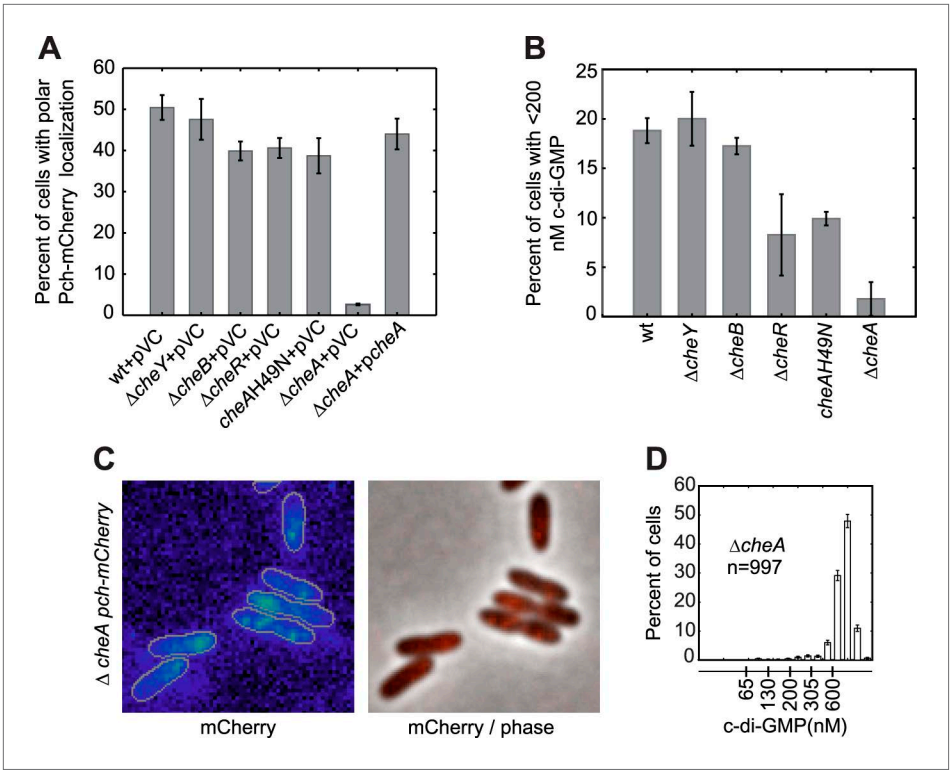

Figure 4. CheA is required for the maintenance of low c-di-GMP and polar localization of Pch-mCherry. (**A**) Quantification of Pch-mCherry polar localization in different *che* mutants. Strains contain empty vector (pVC) or a complementing plasmid. (**B**) Quantification of c-di-GMP in different *che* mutants. Data plotted in (**A**) and (**B**) are from three biological replicates. Error bars in (**A**) and (**B**) depict standard deviation. (**C**) Representative images (10.8 × 10.8 microns) of Pch-mCherry localization in a *cheA* deletion. (**D**) A histogram of cellular c-di-GMP levels in Δ*cheA* cells. Error bars depict the counting error.

DOI: 10.7554/eLife.01402.009

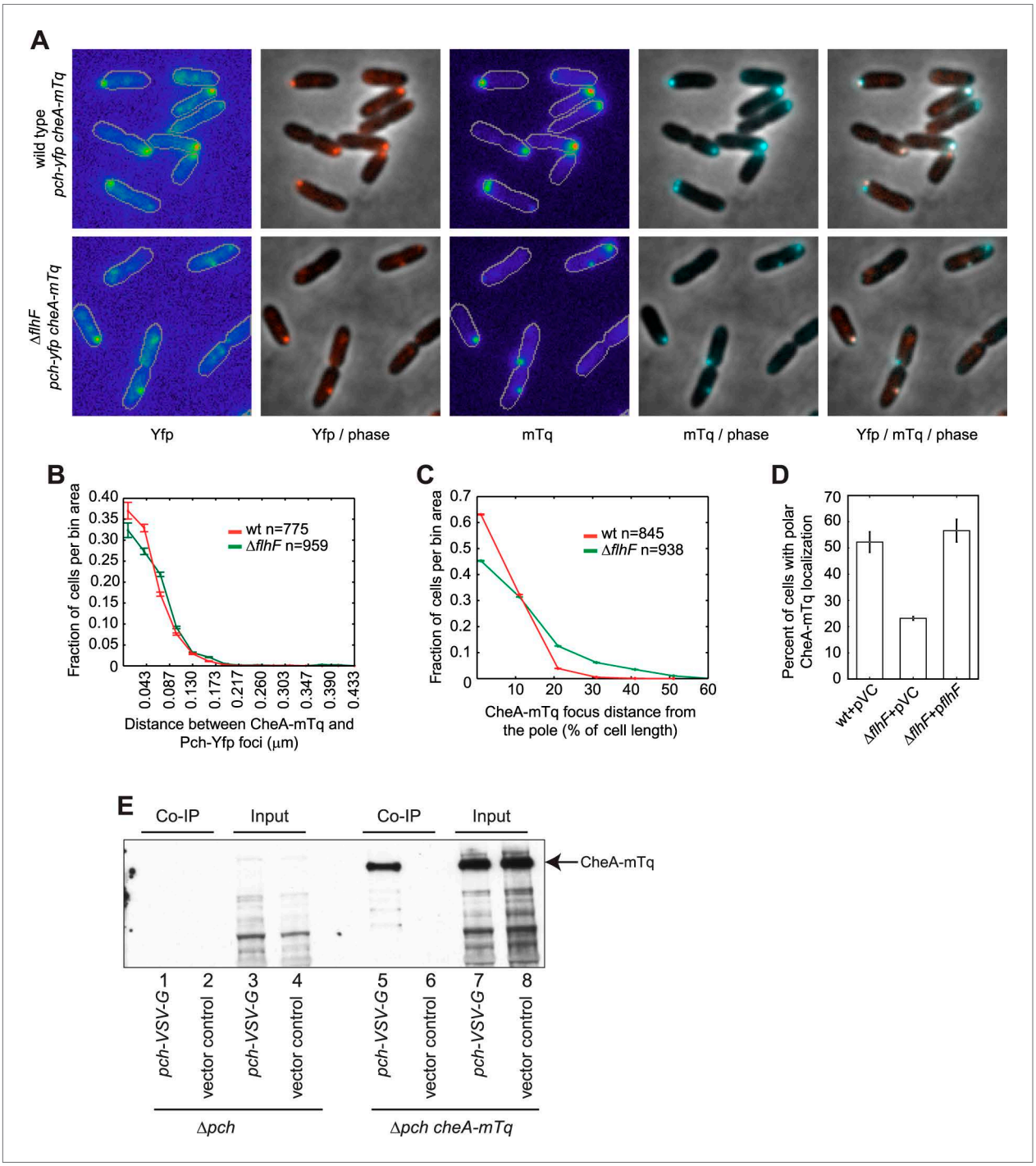

Figure 5. CheA forms a complex with Pch and relies on *flhF* for polar placement. (**A**) Representative images (10.8 × 10.8 microns) of CheA-mTq and Pch-Yfp localization in wild-type (top) and Δ*flhF* (bottom) strains. In the phase/fluorescence channel overlays, CheA-mTq fluorescence is shown in blue and Pch-Yfp fluorescence is shown in red. (**B**) Histogram of the smallest distance between any two CheA-mTq and Pch-Yfp foci in wild-type and Δ*flhF* strain backgrounds. (**C**) Histogram of the CheA-mTq foci distance to the nearest cell pole in wild-type and Δ*flhF* strain backgrounds. In (**B**) and (**C**) error bars depict counting error. (**D**) Percent of cells exhibiting polar localization of CheA-mTq in wild type and Δ*flhF* strain backgrounds from three biological replicates. Strains contain empty vector (pVC) or a complementing plasmid. Error bars depict the standard deviation. (**E**) Co-immunoprecipitation of CheA-mTq and Pch-VSV-G. CheA-mTq of the input lysates and anti VSV-G agarose bead elution fractions was detected by western blot utilizing a monoclonal anti-GFP antibody. Lanes 1–4 show control isolates lacking a CheA-mTq fusion. Lanes 1, 2 and 5, 6 show protein complexes eluted from anti VSV-G agarose beads.

DOI: 10.7554/eLife.01402.010

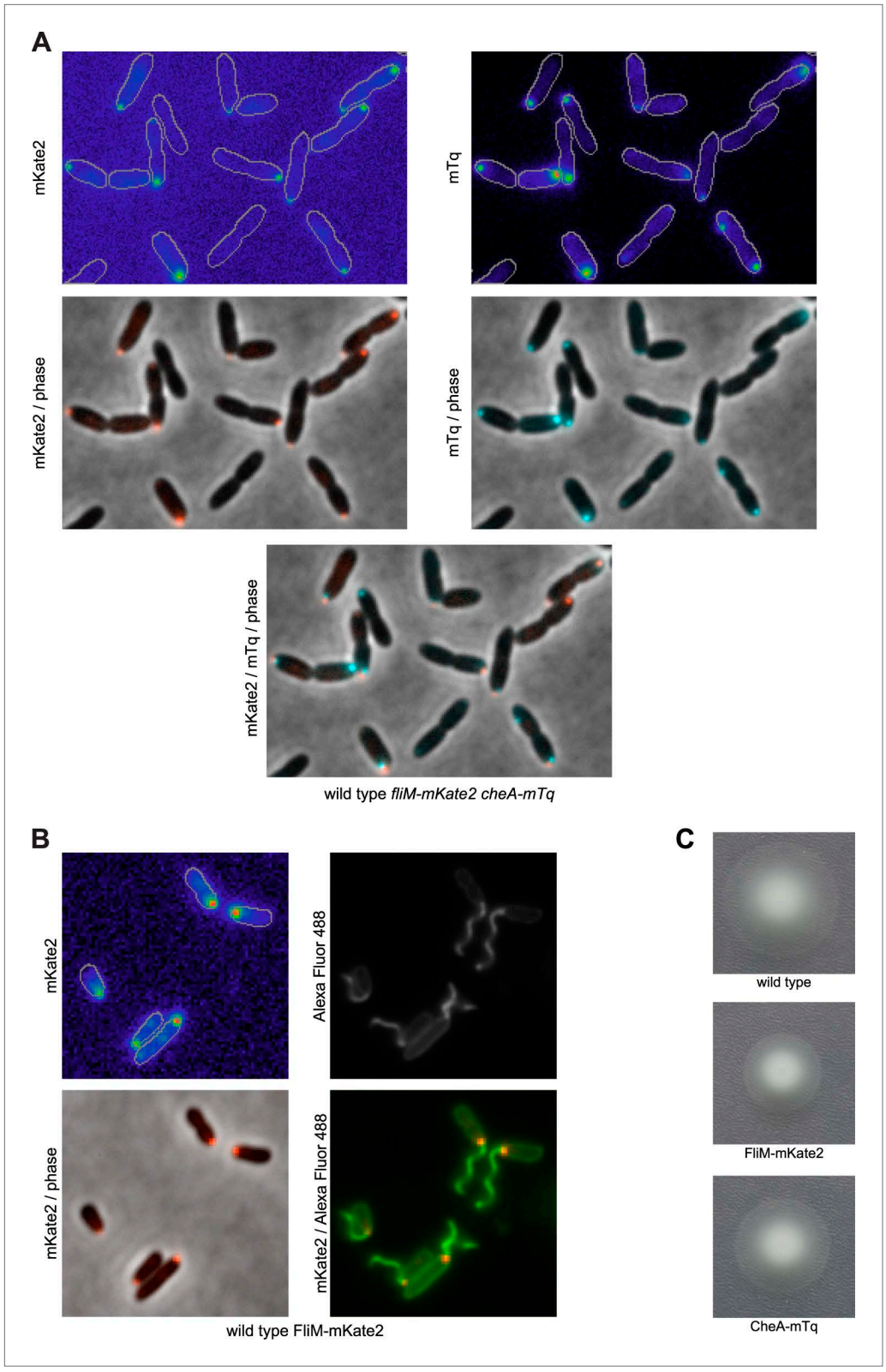

Figure 5—figure supplement 1. CheA localizes to the same pole as FliM. (**A**) Representative images (width of 19.9 microns) of CheA-mTq and FliM-mKate2 subcellular localization. (**B**) FliM-mKate2 does not disrupt flagellar assembly. Representative images (13.1 × 13.1 microns) of FliM-mKate2 localization together with Alexa Fluor 488 labeling of surface exposed amine groups. The bottom left panel shows the overlay of FliM-mKate2 localization (in

Figure 5—figure supplement 1. Continued on next page

Figure 5—figure supplement 1. Continued

red) with the phase contrast image. The bottom right panel shows FliM-mKate2 and amine labeled cells (in green), confirming that the base of the flagellum corresponds to the same location as the FliM-mKate2 focus. The top left panel is of the FliM-mKate2 fluorescence image, and the top right panel is of surface amines labeled with Alexa Fluor 488. (**C**) Bulk motility assays of strains with FliM-mKate2 and CheA-mTq fusions confirm these strains exhibit normal motility and chemotaxis.

DOI: 10.7554/eLife.01402.011

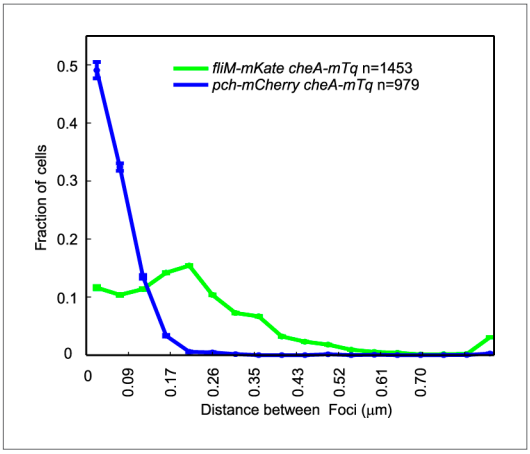

Figure 5—figure supplement 2. CheA-mTq colocalizes with Pch-mCherry but not with FliM-mKate2. A representative histogram of the minimum separation between CheA-mTq and FliM-mKate2 foci and of the minimum separation between CheA-mTq and Pch-mCherry foci. Identical imaging parameters were used for both sets of fluorophore fusions. Error bars depict the counting error.

DOI: 10.7554/eLife.01402.012

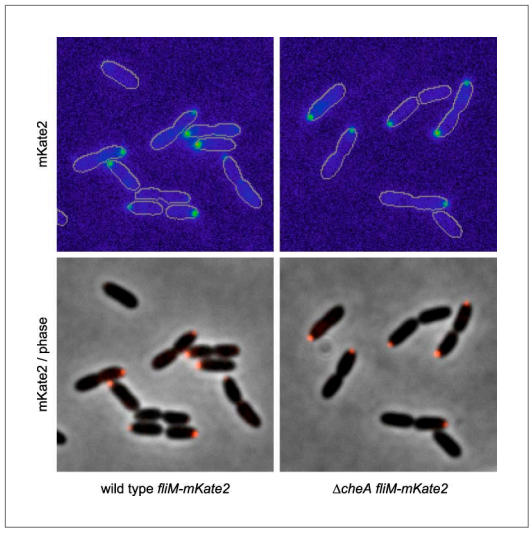

Figure 5—figure supplement 3. FliM-mKate2 polar localization is not dependent upon CheA. Representative images (14.8 microns in width) of FliM-mKate2 localization in wild type and Δ*cheA* backgrounds. From three biological replicates, a mean of 40% (SD of 5%) of wild-type cells exhibit polar localization and 41% (SD of 4%) of Δ*cheA* cells exhibit polar localization.

DOI: 10.7554/eLife.01402.013

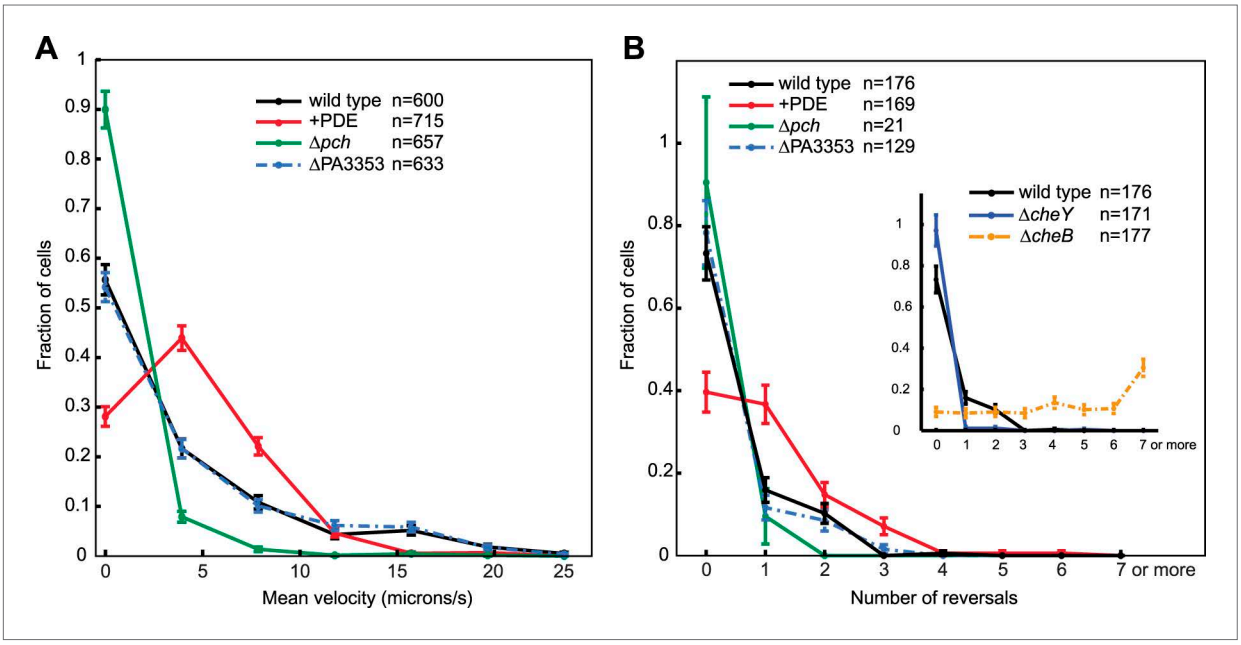

Figure 6. Cells with increased c-di-GMP exhibit decreased velocity and reversals. (**A**) Histogram of mean cellular velocity. The '+PDE' strain uniformly exhibits cellular c-di-GMP concentrations less than 65 nM. (**B**) Histogram of total number of reversals exhibited during 25 micron trajectories. Only cells moving at a velocity of 2 microns/s or greater were analyzed. Reversal data from the control strains are shown in the inset box. The *cheY* deletion is not expected to undergo any reversals. The *cheB* deletion is expected to undergo more reversals than wild type. Error bars depict the counting error. Representative graphs are shown for both (**A**) and (**B**).

DOI: 10.7554/eLife.01402.014